

Shock Regularization with Smoothness-Increasing Accuracy-Conserving Dirac-Delta Polynomial Kernels

B.W. Wissink^{a,d}, G.B. Jacobs^a, J.K. Ryan^b,
W.S. Don^c and E.T.A. van der Weide^d

^a*Department of Aerospace Engineering, San Diego State
University, San Diego, CA*

^b*School of Mathematics, University of East Anglia,
Norwich, UK*

^c*School of Mathematical Sciences, Ocean University
of China, Qingdao, China*

^d*Faculty of Engineering Technology, University of Twente,
Enschede, The Netherlands*

corresponding author, gjacobs@mail.sdsu.edu

September 6, 2021

Abstract

A smoothness-increasing accuracy conserving filtering approach to the regularization of discontinuities is presented for single domain spectral collocation approximations of hyperbolic conservation laws. The filter is based on convolution of a polynomial kernel that approximates a delta-sequence. The kernel combines a k^{th} order smoothness with an arbitrary number of m zero moments. The zero moments ensure a m^{th} order accurate approximation of the delta-sequence to the delta function. Through exact quadrature the projection error of the polynomial kernel on the spectral basis is ensured to be less than the moment error. A number of test cases on the advection equation, Burger's equation and Euler equations in 1D and 2D shown that the filter regularizes discontinuities while preserving high-order resolution.

Keywords

Shock capturing, Hyperbolic conservation laws, Regularization, Dirac-Delta, Chebyshev collocation, Filtering

1 Introduction

Shock capturing with high-order spectral methods is well known to be plagued by Gibbs phenomena in the solution. Nonlinear polynomial reconstruction schemes such as the nonlinear weighted essentially non-oscillatory (WENO) finite difference schemes on a uniformly spaced grid that have been very successful [1] do not extend well to global polynomial based Chebyshev and Legendre collocation (spectral) methods. Since spectral methods rely on high-order global basis functions, slope limiters are often applied to suppress Gibbs's oscillations. The most common approach is to use explicit Runge Kutta Discontinuous Galerkin (RKDG) methods with min-mod slope limiters introduced by Cockburn [2], [3]. A cost-effective alternative to limiting is the artificial viscosity (AV) approach, e.g. [4], [5], [6] where artificial higher even order differential terms are added to the equations to dissipate the high frequency waves or smoothen the small scale structures. While this approach is very stable and more accurate than lower order alternatives, there is no formal proof of higher-order resolution and accuracy. Yet another approach is to use filtering, which has successfully employed in simulating shocked flow [7, 4]. The high order filter used there is the variable order exponential filter, which does not satisfy all the criteria for the definition of filter as laid out in [8] exactly but asymptotically.

A yet to be explored technique for shock capturing is the use of SIAC-like filters. The typical application of SIAC filtering is to obtain superconvergence. This is accomplished by using information that is already contained in the numerical solution to increase the smoothness of the field and to reduce the magnitude of the errors. The solution, as a post-processing step, is convolved against a specifically designed kernel function once at the final time. The foundations for this postprocessor were established by Bramble and Schatz [9]. They showed that the accuracy of Ritz-Galerkin discretizations can be doubled by convolving the solution against a certain kernel function. Cockburn et al. [10] used the ideas of Bramble and Schatz and those of Mock and Lax [11] to demonstrate that the postprocessor is also suitable for DG schemes. They proved that, for a certain class of linear hyperbolic equations with sufficiently smooth solutions, the postprocessor enhances the accuracy from order $k + 1$ to order $2k + 1$ in the L_2 -norm, where k is the polynomial degree of the original DG approximation. This postprocessor relies on a symmetric convolution kernel consisting of $2k + 1$ B-splines of order $k + 1$.

In [12] a regularization technique is developed for the Dirac- δ source terms in hyperbolic equations that is an excellent candidate for a kernel of a SIAC-like regularization filter of shock discontinuities. The technique is based on a class of high-order compactly supported piecewise polynomials introduced in [13]. The piecewise polynomials provide a high-order approximation to the Dirac-Delta whose overall accuracy is controlled by two conditions: the number of vanishing moments and smoothness. SIAC kernels have similar smoothness and moment properties as the Dirac-Delta kernel, but are based on piecewise continuous B-splines instead of polynomials. In [14] it was shown that SIAC-like filters based on the compactly supported Dirac-Delta kernels capture particle-fluid interface discontinuities with higher-order resolution in single domain spectral solutions. The compactness of support is closely related to the moment condition. Smoothness properties yield higher-order resolution away from the discontinuity.

In the present work we have developed SIAC-like filters based on the high-order Dirac-Delta kernel for the regularization of shocks and discontinuities. The filter operation is based on convolution of the solution with the high-order Dirac-Delta kernels. The formulation of the operation is derived and written in matrix-vector multiplication form to allow for an efficient and simple implementation. The filters are tested on a spectral solver for hyperbolic conservation laws, such as the one dimensional scalar linear advection equation and scalar nonlinear Burgers' equation, and both one- and two-dimensional nonlinear Euler equations. We show that, for the case of the linear advection equation, filtering discontinuous initial conditions yields a stable, high-order resolution and with the designed order of accuracy away from the discontinuity.

In the area where the solution is the advected (filtered) initial condition, the designed order of accuracy is achieved and depends on the support width and number of vanishing moments on the kernel. The support width is made proportional to grid-spacing and also depends on the number of vanishing moments.

In the case of the non-linear Burgers' and Euler equations, the filter has to be applied at every time step in order to maintain stability by smoothing shocks and discontinuities during the simulation. This leads to a summation of filter-errors and smearing of the solution near discontinuities. We show that by choosing a sufficiently accurate Dirac-Delta kernel and small support-width, these effects are minimized and design order of accuracy is obtained away from the discontinuity as well.

In Section 2 the filter-operation is derived and background information about SIAC filters, the high-order Dirac-Delta functions and the Chebyshev collocation method is provided. Next, Section 3 presents and discusses the numerical results. Finally, Section 4 summarizes the results and gives an outlook for future work.

2 Formulation and Methodology

2.1 Chebyshev Collocation Method

Polynomial based spectral methods, in this particular case, the Chebyshev collocation method, are commonly used in the discretization of spatial derivatives in PDE's since the order of convergence, for a sufficiently smooth function, depends only on the smoothness of the function, also known as spectral accuracy. For example, the spectral approximation of a C^p function is at least $O(N^{-p})$. In the case of an analytical function, the order of convergence of the approximation is exponential [15]. In the following the Chebyshev collocation method is briefly described for the purpose of introducing notation. For an overview on spectral methods we refer to [15].

The collocation method is based on polynomial interpolation of a function $u(x)$, and can be expressed as

$$u_N(x) = \sum_{j=0}^N u(x_j) l_j(x), \quad l_j(x) = \prod_{k=0, k \neq j}^N \frac{x - x_k}{x_j - x_k}, \quad j = 0, \dots, N, \quad (1)$$

where $x_j, j = 0, \dots, N$ are the collocation points and $l_j(x)$ are the Lagrange interpolation polynomials of degree N . To determine the derivative of the function $u(x)$ at the collocation points x_i , $u'(x_i)$, one can simply take the derivative of the Lagrange interpolating polynomial as

$$\frac{\partial u(x_i)}{\partial x} \approx \sum_{j=0}^N u(x_j) l'_j(x_i). \quad (2)$$

or, written compactly in the matrix-vector multiplication form as

$$\vec{u}' = \mathbf{D} \vec{u}, \quad (3)$$

where the differentiation matrix $D_{i,j} = l'_j(x_i)$. In the case of the Chebyshev collocation method, the collocation points are

$$x_i = -\cos(i\pi/N), \quad i = 0, \dots, N. \quad (4)$$

To integrate the resulting system of ordinary differential equations (ODE) in time, we employ the third order Total Variation Diminishing (TVD) Runge-Kutta scheme

$$\begin{aligned} u^{(1)} &= u^n + \Delta t L(u^n) \\ u^{(2)} &= \frac{3}{4}u^n + \frac{1}{4}u^{(1)} + \frac{1}{4}\Delta t L(u^{(1)}) \\ u^{n+1} &= \frac{1}{3}u^n + \frac{2}{3}u^{(2)} + \frac{2}{3}\Delta t L(u^{(2)}). \end{aligned} \quad (5)$$

2.2 Dirac-Delta Approximation

In [12], a regularization technique based on a class of high-order, compactly supported piecewise polynomials is developed that regularizes the time-dependent, singular Dirac-Delta sources in spectral approximations of hyperbolic conservation laws. This regularization technique provides higher-order accuracy away from the singularity.

For the purpose of clarity in the following discussion, we shall define the compact support domain as $\Omega^\varepsilon = [\varepsilon - x, x + \varepsilon]$ and $\Omega_i^\varepsilon = [x_i - \varepsilon, x_i + \varepsilon]$ centered at $x = x_i$ with a given support width $\varepsilon > 0$.

We shall then define the Dirac-Delta polynomial kernel, denoted as $\delta_\varepsilon^{m,k}(x)$, that is an approximation of the Dirac-Delta function $\delta(x)$,

$$\delta_\varepsilon^{m,k}(x) = \begin{cases} \frac{1}{\varepsilon} P^{m,k}\left(\frac{x}{\varepsilon}\right) & x \in \Omega^\varepsilon, \\ 0 & \text{else,} \end{cases} \quad (6)$$

where $\varepsilon > 0$ is the scaling parameter. The function is generated by a multiplication of two lower degree polynomials that control the number of vanishing moments m , and the number of continuous derivatives at the endpoints of the compact support k , respectively. The $M = m + 2(k + 1)$ degree

polynomial $P^{m,k}(x)$ is uniquely determined by the following properties

$$(P^{m,k})^{(i)}(\pm 1) = 0, \quad i = 1, \dots, k, \quad (7)$$

$$\int_{-1}^1 P^{m,k}(\xi) d\xi = 1, \quad (8)$$

$$\int_{-1}^1 \xi^i P^{m,k}(\xi) d\xi = 0, \quad i = 1, \dots, m, \quad (9)$$

in which (7) determines the number of continuous derivatives at the endpoints (k), (8) states that the function integrates to unity as a Dirac-Delta function, and (9) determines the number of vanishing moments (m). In Fig. 1, we show the polynomial approximation of the Dirac-Delta kernel $\delta_\varepsilon^{m,k}(x)$ with $(m, k) = (3, 8)$ and $(m, k) = (5, 8)$ with scaling parameter $\varepsilon = 1$. It has been shown that the Dirac-Delta approximation $\delta_\varepsilon^{m,k}(x)$ has an accuracy of $O(\varepsilon^{m+1})$.

The procedure for the generation of the polynomials $P^{m,k}(\xi)$ is described in [13]. A few examples for low values of m and k are given below.

- The polynomials with one vanishing moment $m = 1$ and with $k = 0, 1$ and 2 continuous derivatives, respectively, are

$$P^{1,0} = \frac{3}{4}(1 - \xi^2), \quad P^{1,1} = \frac{15}{16}(1 - 2\xi^2 + \xi^4), \quad P^{1,2} = \frac{35}{32}(1 - 3\xi^2 + 3\xi^4 - \xi^6). \quad (10)$$

- The polynomials with three vanishing moments $m = 3$ and with $k = 0, 1$ and 2 continuous derivatives, respectively, are

$$P^{3,0} = \frac{15}{32}(3 - 10\xi^2 + 7\xi^4), \quad P^{3,1} = \frac{105}{64}(1 - 5\xi^2 + 7\xi^4 - 3\xi^6), \quad (11)$$

$$P^{3,2} = \frac{315}{512}(3 - 20\xi^2 + 42\xi^4 - 36\xi^6 + 11\xi^8). \quad (12)$$

2.3 SIAC Filtering

The Smoothness-Increasing Accuracy-Conserving (SIAC) filter was developed in the context of superconvergence extraction and error reduction. SIAC filtering [16, 17, 18, 19] exploits the idea of superconvergence in the underlying method to reduce oscillations in the errors, reduce errors and increase convergence rates. SIAC has its basis in the work by Bramble and Schatz [9] and Cockburn, Luskin, Shu and Süli [10]. It has been extended to include boundary filtering and nonuniform meshes [20, 21, 22, 23, 24] as well as to increase computational efficiency [25, 26]. It has proven effective for applications in visualization [27, 28] and it is expected that this superconvergence extraction technique can act as a natural filter for EFLES.

The traditional application of SIAC filtering takes the numerical approximation, $u_h(x)$, and convolves it against a specially designed kernel,

$$u_h^*(x) = \frac{1}{H} \int_{-\infty}^{\infty} K^{m+1,\ell} \left(\frac{y-x}{H} \right) u_h(y) dy, \quad (13)$$

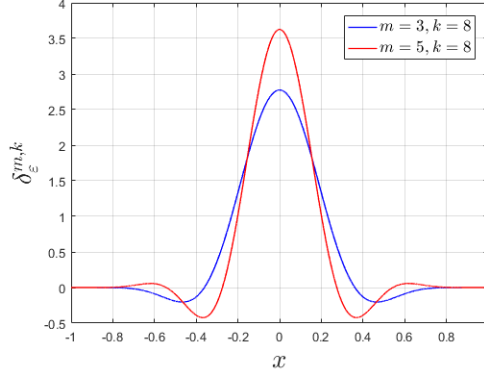


Figure 1: Dirac-Delta kernel $\delta_\varepsilon^{m,k}$ for $(m, k) = (3, 8)$ and $(m, k) = (5, 8)$ with scaling parameter $\varepsilon = 1$.

where $K^{m+1,\ell}$ is a linear combination of m B-splines of order ℓ and H is a scaling typically related to a mesh quantity.

The symmetric form of the post-processing kernel can be written as

$$K^{m+1,\ell}(x) = \sum_{\gamma} c_{\gamma}^{m+1,\ell} \psi^{(\ell)}(x - \gamma), \quad (14)$$

where $\psi^{(\ell)}(x)$ is obtained by convolving the characteristic function over the interval $(-\frac{1}{2}, \frac{1}{2})$ with itself $\ell + 1$ times and the coefficients $c_{\gamma}^{m+1,\ell} \in \mathbb{R}$.

The form of the SIAC kernel is similar to the form of the mixed polynomial [12, 13]. Primary properties of the SIAC that make the SIAC kernel suitable for regularization include:

- $\psi^{(\ell)}(x)$ can be expressed as a linear combination of Delta-functions, using the property $\frac{d^\alpha \psi^{(\ell)}(x)}{dx^\alpha} = \partial_H^\alpha \psi^{(\ell-\alpha)}(x)$, where ∂_H represents a divided difference.
- The SIAC kernel can reproduce polynomials of degree m . This is equivalent to the conditions
 - $\int_{\mathbb{R}} K^{m+1,\ell}(\xi) d\xi = 1$.
 - $\int_{\mathbb{R}} \xi^i K^{m+1,\ell}(\xi) d\xi = 0$ for $i = 1, \dots, m$.

These are similar to the conditions on mixed polynomials. However, unlike the mixed polynomials, the SIAC kernel does not require the smoothness of the kernel even though it vanishes, at the endpoints of the compact support.

2.4 Dirac-Delta Filtering

In [14], an extension from [12], *singular source terms* are expressed as weighted summations of Dirac-Delta kernels that are regularized through approximation theory with convolution operators. The regularization is obtained by convolution with the high-order compactly supported Dirac-Delta

kernel, (6), whose overall accuracy is controlled by the number of vanishing moments m , degree of smoothness k and length of the support ε . In this work, the Dirac-Delta kernel is used to regularize time dependent *discontinuous solutions*. Suppose the solution is given by the variable $u(x)$, $x \in [-1, 1]$. Then the filtered data, $\tilde{u}(x)$, follows from the convolution of $u(x)$ with the Dirac-Delta kernel as

$$\tilde{u}(x) = \int_{-1}^1 u(\tau) \delta_\varepsilon^{m,k}(x - \tau) d\tau. \quad (15)$$

or, simply,

$$\tilde{u}(x) = \int_{\Omega^\varepsilon} u(\tau) \delta_\varepsilon^{m,k}(x - \tau) d\tau, \quad (16)$$

since the Dirac-Delta kernel is zero outside its compact support Ω^ε .

To apply the filtering operation, we need to choose the number of vanishing moments m , the number of continuous derivatives k and the scaling parameter ε .

We make the following notes:

- The number of vanishing moments and support width determine the accuracy of the Delta-kernel and therefore the error introduced by the filtering operation in smooth regions of the solution. In [14] it was proven that the filtering error is $O(\varepsilon^{m+1})$, provided the scaling parameter is $\varepsilon = O(N^{(-k/m+k+2)})$. The requirement on the scaling parameter follows from the fact that the error in the quadrature rule used to evaluate the convolution integral has to be smaller than the $O(\varepsilon^{m+1})$ accuracy of the Dirac-Delta approximation. More vanishing moments reduces the filtering error, however it requires a wider support, leading to a wider regularization zone.
- The smoothness of the Dirac-Delta kernel is controlled by the number of continuous derivatives k at the endpoints. In [14] and [12] it is shown that k controls the smoothness of the transition between the regularized source and the solution and thus controls the order of convergence away from the source. When filtering the entire solution there is no such transition and thus the influence of k is minor. This is confirmed by numerical experiments.

Extension to two dimensions follows straightforwardly from the tensor product of the one-dimensional Delta-function:

$$\delta_\varepsilon^{m,k}(x, y) = \delta_\varepsilon^{m,k}(x) \otimes \delta_\varepsilon^{m,k}(y) \quad (17)$$

Fig. 2 shows the two-dimensional equivalents of the one-dimensional kernels shown in Fig. 1. As in the one-dimensional case, the filtering is based on the convolution of the solution with the Delta-kernel,

$$\tilde{u}(x, y) = \int_{\Omega_x^\varepsilon} \int_{\Omega_y^\varepsilon} u(\tau, \eta) \delta_\varepsilon^{m,k}(x - \tau, y - \eta) d\tau d\eta. \quad (18)$$

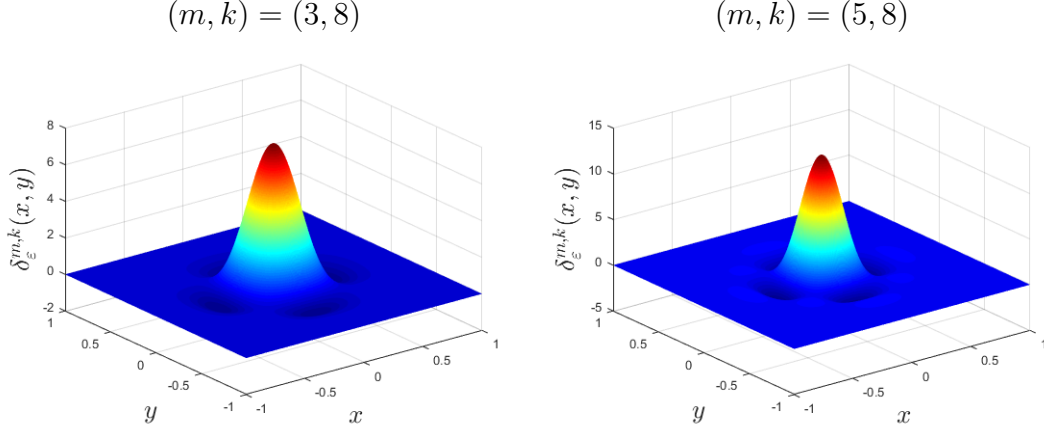


Figure 2: (Color online) Tensor product of the one-dimensional Dirac-Delta function, for (Left) $(m, k) = (3, 8)$ and (Right) $(m, k) = (5, 8)$ with scaling parameter $\varepsilon = 1$.

2.5 Implementation of the Filtering Operation

Filtering of the interpolant of the solution (1), leads to,

$$\tilde{u}_N(x) = \int_{\Omega^\varepsilon} \left[\sum_{i=0}^N u(x_i) l_i(\tau) \right] \delta_\varepsilon^{m,k}(x - \tau) d\tau = \sum_{i=0}^N u(x_i) S_i(x), \quad (19)$$

after interchanging the summation and integration, where the filtering function $S_i(x)$ is

$$S_i(x) = \int_{\Omega^\varepsilon} l_i(\tau) \delta_\varepsilon^{m,k}(x - \tau) d\tau. \quad (20)$$

Hence, one has, at the collocation points,

$$\vec{\tilde{u}} = \mathbf{S} \vec{u}, \quad (21)$$

where the $(N + 1) \times (N + 1)$ filtering matrix \mathbf{S} has elements

$$S_{i,j} = \int_{\Omega_j^\varepsilon} l_i(\tau) \delta_\varepsilon^{m,k}(x_j - \tau) d\tau. \quad (22)$$

In two dimensions, the filtering operation can be written compactly as

$$\tilde{\mathbf{U}} = \mathbf{S}_x \mathbf{U} \mathbf{S}_y^T, \quad (23)$$

where \mathbf{S}_x and \mathbf{S}_y are the one-dimensional filtering matrix in x - and y - direction respectively and the superscript T denotes transpose.

Remark 1 *Near the boundaries, the compact support of the high-order Dirac-Delta function, $\delta_\varepsilon^{m,k}$, extends out of the domain and hence, the data can not be filtered in that case. This means that $\tilde{u}(x) = u(x)$ for $|x| > 1 - \varepsilon$. The filtering matrix S can be precomputed and stored for later use as long as the filter parameters remain unchanged.*

2.6 Clenshaw-Curtis quadrature

The one remaining important issue that needs to be addressed is how to evaluate the integrals in Eq. 19. Since the high-order Dirac-Delta function is a polynomial of degree $M = m + 2(k + 1)$ and the Lagrange interpolation polynomial is of degree $N - 1$, the integrand is a polynomial of degree $M + N - 1$ and can be evaluated analytically. Since this can become time-consuming for large N an appropriate quadrature rule is preferred. For this purpose Clenshaw-Curtis quadrature will be used, that is,

$$\int_{\Omega_i^\varepsilon} l_n(\tau) \delta_\varepsilon^{m,k}(x_i - \tau) d\tau \approx \sum_{q=0}^Q w_q l_n(x_q) \delta_\varepsilon^{m,k}(x_i - x_q). \quad (24)$$

where Q is the number of Chebyshev Gauss-Lobatto quadrature nodes used in the compact support domain Ω_i^ε , that is,

$$x_q = x_i - \varepsilon \cos\left(\frac{\pi q}{Q}\right), \quad q = 0, \dots, Q, \quad (25)$$

and w_q are the corresponding weights. Clenshaw Curtis quadrature exactly evaluates polynomials of degree $Q - 1$. Hence, if one takes $Q = M + N$, the integrals are evaluated exactly. Also, the weights w_q can be precomputed using fast Fourier transform (FFT).

2.7 Shock Capturing with Dirac-Delta Filtering

The theoretical requirement for the scaling parameter, $\varepsilon = \mathcal{O}(N^{-(k/m+k+2)})$, to assure $\mathcal{O}(\varepsilon^{m+1})$ accuracy in the convolution operation is based on the requirement that the error in the quadrature rule has to be smaller than the error in the Dirac-Delta approximation [14]. Since the convolution integrals in this work are solved exactly using Clenshaw-Curtis quadrature, this criterium can be relaxed. For shock capturing we choose the scaling parameter to be proportional to the grid spacing and to guarantee that a minimal of at least two neighboring collocation points will be located inside the compact support width Ω_i^ε for any point $x = x_i$. In this case, the scaling parameter will be expressed in terms of the number of points N_d the kernel spans at the center of the domain $x = x_{N/2}$, assuming N is even, that is,

$$\varepsilon = \sin(\pi N_d / (2N)). \quad (26)$$

The value of N_d is determined empirically and chosen to ensure stable converging results. It depends on the number of vanishing moments m of the Dirac-Delta kernel and whether the filter is applied in a linear or non-linear equation. For implementation in the linear advection equation, only the initial condition is filtered while for a nonlinear PDE's, such as the Burgers' equation and the Euler equations, the solution is filtered at every Runge Kutta time step. This is because of the formation of a finite space-time singularity by the nonlinearity of the equations. However, filtering can lead to smearing of the discontinuity and the summation of filter errors in smooth regions. In order to limit these less desirable effects, we use a smaller scaling parameter, ε , as compared to the linear advection equation.

Remark 2 *Near the boundary the filter cannot be convoluted due to the symmetry of the convolution kernel. In this paper those few points are reset to be the exact solution for the nonlinear PDEs in order to isolate and study solely the effects of the Dirac-Delta kernels. Furthermore, to avoid the effect of variable time step Δt , we fixed the stable time step of $\Delta t = 1 \times 10^{-5}$ in all the simulations performed below in order to be able to compare results.*

3 Numerical Tests

3.1 Advection equation

We shall consider the simple one-dimensional linear advection equation with a discontinuity as initial condition on the domain $-1 < x < 1$,

$$\begin{aligned} \frac{\partial u}{\partial t} + \frac{\partial u}{\partial x} &= 0, \\ u(x, 0) &= \begin{cases} \sin(\pi x) - 0.5 & x \leq -0.25 \\ \sin(\pi x) + 0.5 & x > -0.25 \end{cases}, \\ u(-1, t) &= \sin(\pi(-1 - t)) - 0.5. \end{aligned} \tag{27}$$

The initial condition is first filtered by the filtering matrix \mathbf{S} . For the results below we used a Dirac-Delta kernel with $(m, k) = (3, 8)$ and $N_d = 13$.

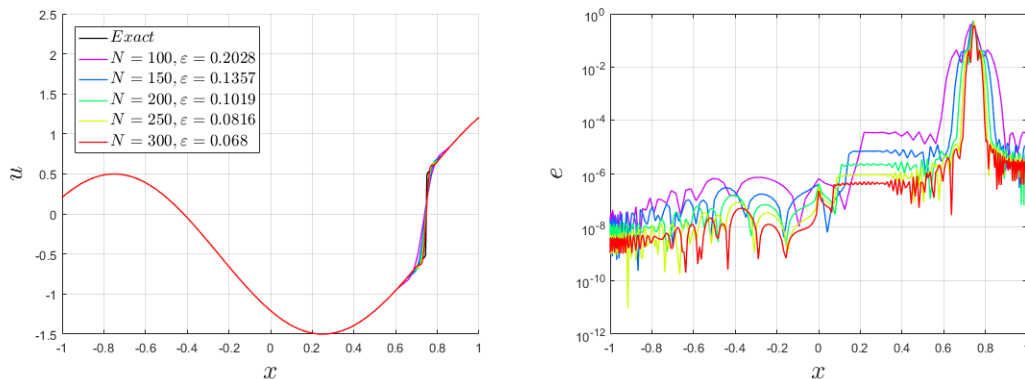


Figure 3: Linear advection equation: Analytical and spectral solution (Left), and pointwise error (Right) at time $t = 1$, for the five different grids with $(m, k) = (3, 8)$ and $N_d = 13$.

In Fig. 3, the point-wise error clearly shows the advected filter error for $x > 0$ caused by filtering the initial condition. In Fig. 4, the rate of convergence outside the regularization zone is examined at $x = 0.28$ and follows the theoretical value of $O(\varepsilon^{m+1})$.

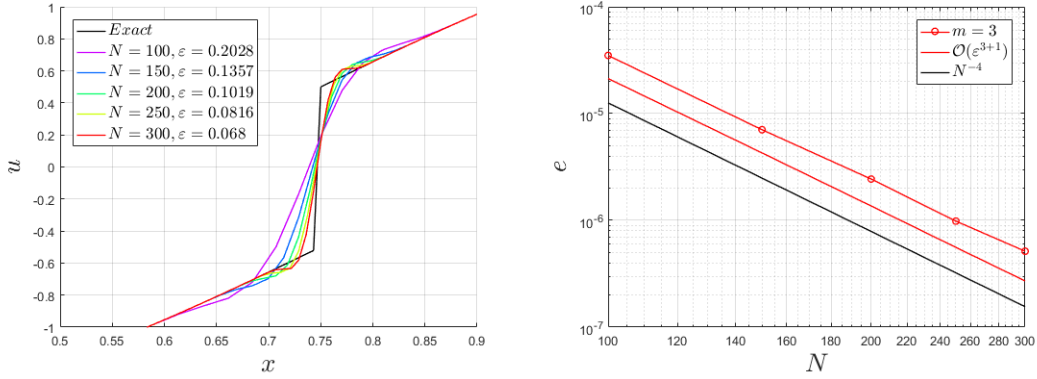


Figure 4: Linear advection equation: Detail view of regularization zone (Left) and error convergence at $x = 0.28$ compared to the theoretical value $O(\varepsilon^{m+1})$ (Right) for the five different grids with $(m, k) = (3, 8)$ and $N_d = 13$.

3.2 Burger's equation

Next, we consider the Burgers' equation,

$$\frac{\partial u}{\partial t} + \frac{1}{2} \frac{\partial u^2}{\partial x} = 0, \quad (28)$$

$$u(x, 0) = -\sin(\pi x), \quad (29)$$

$$u(\pm 1, t) = 0$$

In this case, the solution is filtered at the end of every Runge-Kutta time step. For the results below we used a kernel with $(m, k) = (3, 8)$ and $N_d = 2.5$.

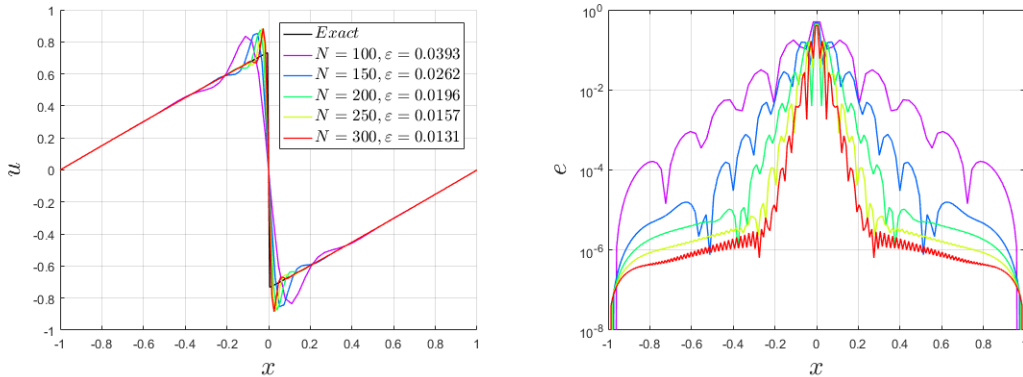


Figure 5: Burger's equation: Analytical and spectral solution (Left), and pointwise error (Right) at time $t = 1$, for the five different grids with $(m, k) = (3, 8)$ and $N_d = 2.5$.

The solution in Figure 5 shows that the filtering effectively captures the shock and gives a stable

solution. A clearly visible overshoot is however introduced. Because of the non-linear character of the solution, increasing the number of vanishing moments does improve the result.

The error (Fig. 5) that is introduced by regularization at the shock location is smeared over the domain by the multiple application of the filter at each time step. For the values of N_d used here, the smearing is small. The smearing effect increases with increasing support width. We note that extending the simulation time until $t = 5$ does not change the error much as compared to error at $t = 1$. Only the shock is slightly more dissipated.

3.3 Euler equations

The 2D unsteady Euler Equations in conservative form are given as

$$\frac{\partial U}{\partial t} + \frac{\partial F_x}{\partial x} + \frac{\partial F_y}{\partial y} = 0, \quad (30)$$

where the conserved quantities U and the flux vectors F_x and F_y are given by

$$U = \begin{pmatrix} \rho \\ \rho u \\ \rho v \\ \rho E \end{pmatrix}, F_x = \begin{pmatrix} \rho u \\ \rho u^2 + p \\ \rho uv \\ (\rho E + p)u \end{pmatrix}, F_y = \begin{pmatrix} \rho v \\ \rho uv \\ \rho v^2 + p \\ (\rho E + p)v \end{pmatrix}. \quad (31)$$

The system is closed by assuming a calorically perfect gas, which relates the pressure to the density, velocity and energy. For the two-dimensional case this gives

$$p = (\gamma - 1) \left(\rho E - \frac{1}{2} \rho (u^2 + v^2) \right), \quad (32)$$

in which γ is the specific heat ratio, which is 1.4 for air.

3.3.1 Sod's shock tube problem

Sod's shock tube problem is governed by the 1D Euler equations. The initial conditions for Sod's shock tube problem are

$$\begin{aligned} \rho_L &= 1.0 & \rho_R &= 0.125, \\ p_L &= 1.0 & p_R &= 0.1, \\ u_L &= 0.0 & u_R &= 0.0. \end{aligned}$$

where the left state is in the domain with $x < 0$ and the right state is in $x \geq 0$. The conserved quantities are filtered every time-step using the filtering matrix. For the results below we used a kernel with $(m, k) = (3, 8)$ and $N_d = 2.5$. The solutions show that both the shock and the contact discontinuity are effectively captured using the filter-operation. A low error is observed outside the regularization zone.

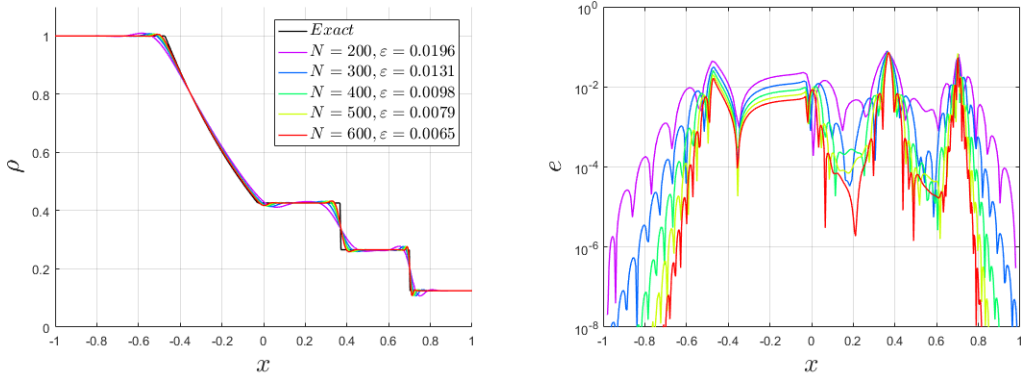


Figure 6: Analytical solution, spectral solution (Left) and pointwise error (Right) of the density at $t = 0.4$, for the five different grids for $(m, k) = (3, 8)$ and $N_d = 2.5$.

3.3.2 Shu-Osher problem

Shu-Osher's Problem is also governed by the 1D Euler equations with the initial conditions of the primitive variables in the left state $(\rho_L, P_L, u_L) = (27/7, 31/3, 4\sqrt{35}/9)$ and the right state $(\rho_R, P_R, u_R) = (1 + 0.2 \sin(25x), 1, 0)$. Again, the conserved quantities are filtered every time-step using the filtering matrix. For the results below we used a kernel with $(m, k) = (5, 8)$ and $N_d = 5.5$ in order to limit the error introduced in the entropy-wave. A 5th order WENO-solution on 10000 points is used to serve as a reference 'exact' solution.

Results, $\delta_\varepsilon^{5,8}$, $N_d = 6.5$

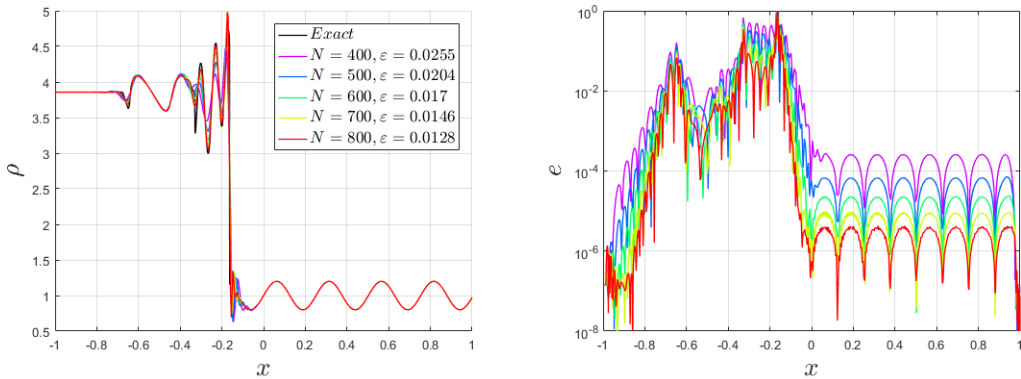


Figure 7: Analytical solution, spectral solution (Left) and pointwise error (Right) of the density at $t = 0.18$, for the five different grids for $(m, k) = (5, 8)$ and $N_d = 6.5$.

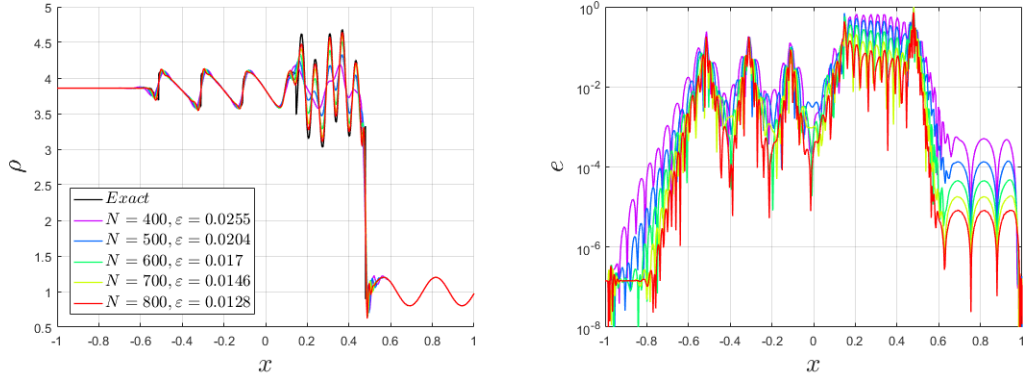


Figure 8: Analytical solution, spectral solution (Left) and pointwise error (Right) of the density at $t = 0.36$, for the five different grids for $(m, k) = (5, 8)$ and $N_d = 6.5$.

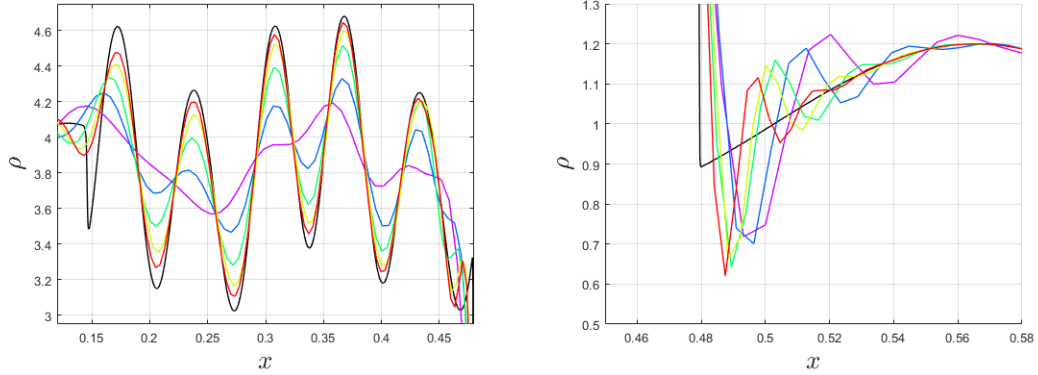


Figure 9: Detail view of the entropy wave (Left) and the regularization zone (Right) at $t = 0.36$, for the five different grids for $(m, k) = (5, 8)$ and $N_d = 6.5$.

The solution shows that the filter effectively captures the shock while the kernel with $m = 5$ vanishing moments ensures high resolution behind the shock. Fig. 9 provides a detail view of the entropy wave (Left) and the regularization zone (Right).

3.4 Explosion problem

As a 2D test case, the explosion problem is considered. This problem is governed by the 2D Euler equations, (30), (31) and (32). The equations are solved on a 2.0×2.0 square domain in the $x - y$ plane. The initial condition consists of the region inside of a circle with radius $R = 0.4$ centered at $(0, 0)$ and the region outside of the circle. The flow variables are constant in each of these regions

and are separated by a circular discontinuity at time $t = 0$. The two constant states are chosen as:

$$\rho_{in} = 1.0 \quad \rho_{out} = 0.125, \quad (33)$$

$$p_{in} = 1.0 \quad p_{out} = 0.1, \quad (34)$$

$$u_{in} = 0.0 \quad u_{out} = 0.0, \quad (35)$$

$$v_{in} = 0.0 \quad v_{out} = 0.0, \quad (36)$$

where the subscripts *in* and *out* denote values inside and outside the circle, respectively. The approach described by Eleuterio [29] is used to serve as an exact solution. For the results below we used a kernel with $(m, k) = (3, 8)$ and $N_d = 2.5$.

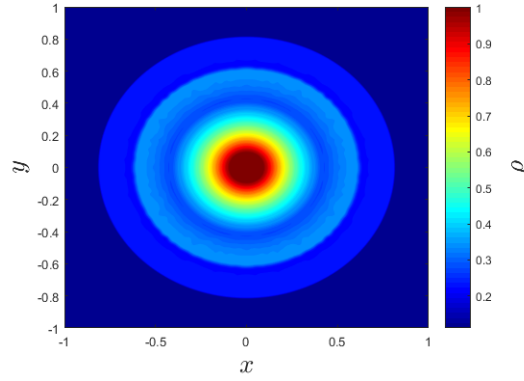


Figure 10: Contour plot of the density at $t = 0.25$ for $(m, k) = (3, 8)$ and $N_d = 2.5$.

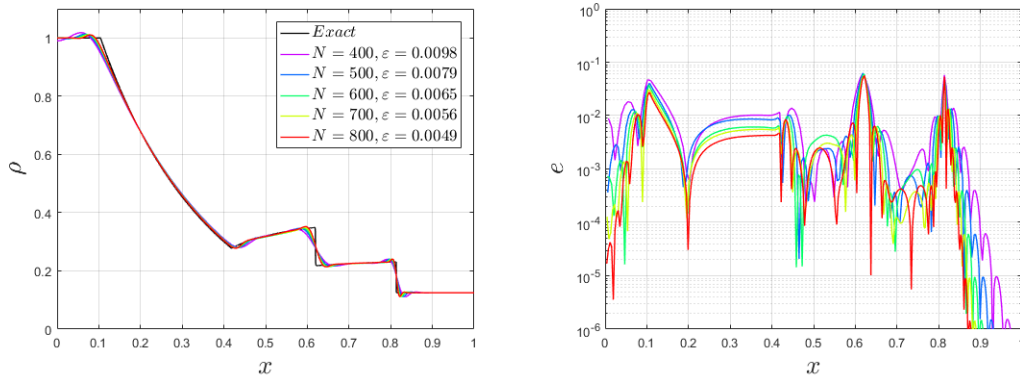


Figure 11: Numerical solution (Left) and error (Right) along the radial line at $t = 0.25$, for the five different grids for $(m, k) = (3, 8)$ and $N_d = 2.5$.

The contour plot of the density shows that the symmetry of the flow is captured on the 2D Cartesian grid. Comparisons along any radial line give identical results.

4 Conclusions and future work

In this paper, the use of high-order Dirac-Delta function based filters for the regularization of shocks and discontinuities in combination with a global spectral method is investigated. We have shown that these filters are able to effectively capture shocks while maintaining high resolution in smooth areas of the solution.

As a first next step for future work, the filtering operation has to be extended for the use in discontinuous spectral element methods. Furthermore the development of a way to apply the filtering near the boundaries is desired. A possible way could be the development of special one-sided polynomial kernels, analog to the one-sided SIAC kernels for boundary filtering [28], [20].

In the present work, the developed filters have been applied globally, i.e. the whole domain is affected by the filter, thus causing (small) errors in smooth areas and smearing of the discontinuity. It would be beneficial if this effect could be limited. This could be accomplished if only the area of the discontinuity is filtered. This however requires some means to identify shocks and discontinuities in the solution. One possibility is the use of multi-resolution analysis (MR) [30], [31]. MR-analysis is successfully used in hybrid spectral-WENO methods to switch between high-resolution WENO methods for shocked regions and computationally efficient spectral methods in smooth regions [32]. In a follow on paper, we intend to report on the use the filter-error itself to identify shocks and discontinuities. The filter-error

$$e = |\mathbf{u} - \mathbf{S}\mathbf{u}|, \quad (37)$$

describes the shape of the solution in the sense that it is small in smooth areas and large in shocked areas. If a function $L(e)$ can be derived that is able to determine which areas should be filtered and which not, the filtering operation could be improved and implemented according to

$$\tilde{\mathbf{u}} = L(e)\mathbf{u} + (1 - L(e))\mathbf{S}\mathbf{u}. \quad (38)$$

Thus for areas in which $L(e) = 1$ the solution is not filtered whereas if $L(e) = 0$ the solution is fully filtered. This would then effectively limit the smearing and the error introduced in smooth areas.

References

- [1] C.W. Shu and S. Osher. Efficient Implementation of Essentially Non-oscillatory Shock-Capturing Schemes. *Journal of Computational Physics*, 77:439–471, 1988.
- [2] B. Cockburn. Devising discontinuous galerkin methods for non-linear hyperbolic conservation laws. *J. Comp. Appl. Math.*, 128:187–204, 2001.
- [3] B. Cockburn and C.W. Shu. Runge-kutta discontinuous galerkin methods for convection-dominated problems. *Journal of scientific computing*, 16:173–261, 2001.
- [4] A. Chaudhuri, G.B. Jacobs, W.S. Don, H. Abassi, and F. Mashayek. Explicit discontinuous spectral element method with entropy generation based artificial viscosity for shocked viscous flows. *J. Comp. Phys.*, 332:99–117, 2017.

- [5] T.J. Hughes, L. Franca, and M. Mallet. A new finite element formulation for computational fluid dynamics: I. symmetric forms of the compressible euler and navier-stokes equations and the second law of thermodynamics. *Computer Methods in Applied Mechanics and Engineering*, 54:223–234, 1986.
- [6] J.L. Guermond, R. Pasquetti, and B. Popov. Entropy viscosity method for nonlinear conservation laws. *Journal of Computational Physics*, 230:4248–4267, 2011.
- [7] W.S. Don. Numerical Study of Pseudospectral Methods in Shock Wave Applications. *J. Comput. Phys.*, 110:103–111, 1994.
- [8] H. Vandeven. Family of spectral filters for discontinuous problems. *Journal of Scientific Computing*, 6(2):159–192, 1991.
- [9] J.H. Bramble and A.H. Schatz. Higher Order Local Accuracy by Averaging in the Finite Element Method. *Mathematics of Computation*, 31:94–111, 1977.
- [10] B. Cockburn, M. Luskin, C.W. Shu, and E. Sli. Enhanced Accuracy by Post-processing for Finite Element Methods for Hyperbolic Equations. *Mathematics of Computation*, 72:577–606, 2003.
- [11] M.S. Mock and P.D. Lax. The computation of discontinuous solutions of linear hyperbolic equations. *Comm. Pure Appl. Math.*, 18:423–430, 1978.
- [12] J.P. Suarez, G.B. Jacobs, and W.S. Don. A high-order Dirac-delta regularization with optimal scaling in the spectral solution of one-dimensional singular hyperbolic conservation laws. *SIAM J. Sci. Comp*, 36:1831–1849, 2014.
- [13] A.K. Tornberg. Multi-dimensional quadrature of singular and discontinuous functions. *BIT*, 42:644–669, 2002.
- [14] J.P. Suarez and G.B. Jacobs. Regularization of singularities in the weighted summation of Dirac-delta functions for the spectral solution of hyperbolic conservation laws. *J. Sci. Comp.*, preprint at: <https://arxiv.org/abs/1611.05510>.
- [15] Sigal Gottlieb Jan Hesthaven and David Gottlieb. Spectral Methods for Time-Dependent Problems. *Cambridge University Press, Cambridge, United Kingdom*.
- [16] J.K. Ryan, C.W. Shu, and H.L. Atkins. Extension of a post-processing technique for discontinuous Galerkin methods for hyperbolic equations with application to an aeroacoustic problem. *SIAM Journal on Scientific Computing*, 26:821–843, 2004.
- [17] J. King, H. Mirzaee, J.K. Ryan, and R.M. Kirby. Smoothness-Increasing Accuracy-Conserving (SIAC) filtering for discontinuous Galerkin solutions: Improved errors versus higher-order accuracy. *Journal of Scientific Computing*, 53:129–149, 2012.
- [18] S. Curtis, R.M. Kirby, J.K. Ryan, and C.W. Shu. Post-processing for the discontinuous Galerkin method over non-uniform meshes. *SIAM Journal on Scientific Computing*, 30:272–289, 2007.

- [19] L. Ji, P. van Slingerland, J.K. Ryan, and C. Vuik. Superconvergent error estimates for a position-dependent Smoothness-Increasing Accuracy-Conserving filter for DG solutions. *Mathematics of Computation*, 83:2239–2262, 2014.
- [20] J.K. Ryan and C.W. Shu. On a one-sided post-processing technique for the discontinuous Galerkin methods. *Methods Appl. Anal.*, 10:295–307, 2003.
- [21] P. van Slingerland, J.K. Ryan, and C. Vuik. Position-dependent Smoothness-Increasing Accuracy-Conserving (SIAC) filtering for accuracy for improving discontinuous Galerkin solutions. *SIAM J. Sci. Comp.*, 33:802–825, 2011.
- [22] X. Li, R.M. Kirby, and C. Vuik. Computationally efficient position-dependent Smoothness-Increasing Accuracy-Conserving (SIAC) filtering: The uniform mesh case. *Preprint*, 2013.
- [23] X. Li, R.M. Kirby, and C. Vuik. Computationally efficient position-dependent Smoothness-Increasing Accuracy-Conserving (SIAC) filtering: The nonuniform mesh case. *Preprint*, 2014.
- [24] H. Mirzaee, L. Ji, J.K. Ryan, and R.M. Kirby. Smoothness-Increasing Accuracy-Conserving (SIAC) post-processing for discontinuous Galerkin solutions over structured triangular meshes. *SIAM Journal on Numerical Analysis*, 49:1899–1920, 2011.
- [25] H. Mirzaee, J.K. Ryan, and R.M. Kirby. Quantification of errors introduced in the numerical approximation and implementation of Smoothness-Increasing Accuracy-Conserving (SIAC) filtering of discontinuous Galerkin (DG) fields. *Journal of Scientific Computing*, 45:447–470, 2010.
- [26] H. Mirzaee, J.K. Ryan, and R.M. Kirby. Efficient implementation of Smoothness-Increasing Accuracy-Conserving (SIAC) filters for discontinuous Galerkin solutions. *Journal of Scientific Computing*, 52:85–112, 2012.
- [27] M. Steffan, S. Curtis, R.M. Kirby, and J.K. Ryan. Investigation of Smoothness-Increasing Accuracy-Conserving Filters for Improving Streamline Integration through Discontinuous Fields. *IEEE-TVCG*, 14:680–692, 2008.
- [28] D. Walfisch, J.K. Ryan, R.M. Kirby, and R. Haimes. One-sided Smoothness-Increasing Accuracy-Conserving filtering for enhanced streamline integration through discontinuous fields. *Journal of Scientific Computing*, 38:164–184, 2009.
- [29] Eleuterio F. Toro. Riemann Solvers and Numerical Methods for Fluid Dynamics. *Springer-Verlag, Berlin*, 2009.
- [30] A. Harten. High resolution schemes for hyperbolic conservation laws. *Comput. Phys.*, 49:357–393, 1983.
- [31] A. Harten. Adaptive multiresolution schemes for shock computations. *Comput. Phys.*, 115:319–338, 1994.
- [32] B. Costa and W.S. Don. Multi-domain hybrid spectral-WENO methods for hyperbolic conservation laws. *Journal of Computational Physics*, 224:970–991, 2007.